

# Improving visibility in photoacoustic imaging using dynamic speckle illumination

Jérôme Gateau, Thomas Chaigne, Ori Katz, Sylvain Gigan and Emmanuel Bossy\*

*Institut Langevin, ESPCI ParisTech, CNRS UMR 7587, INSERM U979, 1 rue Jussieu, 75005 Paris, France*

*\*Corresponding author: emmanuel.bossy@espci.fr*

In high-frequency photoacoustic imaging with uniform illumination, homogenous photo-absorbing structures may be invisible because of their large size or limited-view issues. Here we show that it is possible to reveal features, which are normally invisible with a photoacoustic system comprised of a 20MHz linear ultrasound array, by exploiting dynamic speckle illumination. We demonstrate imaging of a  $\emptyset 5\text{mm}$  absorbing cylinder and a  $30\mu\text{m}$  black thread arranged in a complex shape. The hidden structures are directly retrieved from photoacoustic images recorded for different random speckle illuminations of the phantoms by assessing the variation in the value of each pixel over the illumination patterns.

In biomedical imaging, randomly distributed sub-resolution sources or scatterers usually result in speckle artifacts. In ultrasonography, acoustic speckle is of primary importance for characterization of soft tissue [1] as it enables to visualize large or complex-shaped structures comprised of unresolved scatterers, even when they are densely packed. On the other hand, photoacoustic imaging is known to be mostly speckle-free for uniform illumination and large density of optical absorbers contained in structures with smooth boundaries [2]; blood vessels filled with hemoglobin for instance. The lack of acoustic speckle artifacts in photoacoustics has been attributed to the strong initial phase correlation among the ultrasound waves generated by the individual absorbing molecules or particles after quasi-instantaneous optical excitation. Two related effects of this correlation are the directivity of the ultrasonic emission for elongated structures and the prominent boundary build up for large structures. This results in visibility issues when imaging homogeneous structures using a photoacoustic system with uniform illumination, because of the limited bandwidth and/or the limited view of practical implementations [3].

To address this visibility problem, we propose here to exploit optical speckle patterns naturally present in coherent illumination as a source of structured illumination, effectively breaking the homogeneity of absorbing structures and rendering them visible in photoacoustic imaging. Dynamic speckle illumination has proved very useful in optical microscopy for optical sectioning [4], and was recently also exploited as a structured illumination source to surpass the optical diffraction limit [5]. As photoacoustic techniques aim at imaging beyond the depth achieved by optical microscopy [6], only random a-priori unknown structured illumination provided by the passage of coherent light through a scattering medium can be considered.

In the present study, unlike in conventional photoacoustic imaging where a locally uniform illumination is assumed, we investigate the operation of a

high frequency and limited-view photoacoustic system with dynamic optical speckle illumination of homogeneously absorbing structures. The final images are obtained by computing the local variations of the signal under the different speckle illumination.

The experimental set-up is illustrated in Fig. 1(a). Optical excitation was performed with a Q-Switched Nd:YAG oscillator laser (Brilliant, Quantel) delivering 4ns duration pulses at  $\lambda_{\text{laser}}=532\text{nm}$  with a 10 Hz repetition rate, and a coherence length on the order of 1mm. To generate the varying speckle illumination, the laser beam was passed through a ground glass diffuser (220 Grit, Thorlabs), mounted on a rotation mount. The rotating diffuser acted here as a random inhomogenous dynamic medium producing temporally varying speckle patterns with no appreciable ballistic transmitted component, just like a thick scattering biological tissue would. The main difference is the scattering induced path-length differences. Path-length differences larger than the laser coherence length may reduce speckle contrast, and were avoided here by employing a thin scattering layer.

The diffuser was positioned at a distance  $L=15\text{ mm}$  to  $150\text{ mm}$  from the imaged plane of the sample. Varying this distance allowed to control the optical speckle grain size on the target plane, which is given by:  $D_{\text{speckle}} \propto \lambda_{\text{laser}} L / D_{\text{beam}}$ , where  $D_{\text{beam}} \sim 6\text{mm}$  is the diameter of the laser input beam impinging on the diffuser surface [7]. In our experiments  $L$  was varied to produce speckle grain

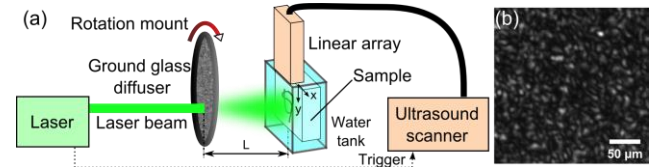


Fig.1: (a) Schematic of the experimental setup. The distance  $L$  corresponds to the distance between the incident surface of the diffuser and the imaging plane. A coordinate system is introduced for the imaging plane. Its origin is the middle point of the array. (b) A typical optical speckle pattern recorded with the camera in the  $xy$  plane (grain size of  $6.3\text{ }\mu\text{m} \pm 0.8\text{ }\mu\text{m}$ ).

sizes ranging from  $D_{\text{speckle}} = 2.6\mu\text{m} \pm 0.6\mu\text{m}$  to  $18.3\mu\text{m} \pm 1.7\mu\text{m}$ . The speckle grain size was determined prior to the photoacoustic experiments by imaging the optical field on a camera (Manta G-046, Allied Vision Technologies) [Fig. 1(b)], and calculating the  $1/e^2$  radius of the normalized spatial autocorrelation function of the optical speckle image.

Two samples were prepared to mimic the most common artifacts in high-frequency photoacoustic imaging: boundary build-up [2] [Fig. 2] and limited view [8] [Fig. 3], and to verify the benefits of our technique. Both samples were imaging phantoms comprised of homogenous photoabsorbing structures embedded in 1.5%w/v agarose gel (A9539, Sigma). The gel supporting the sample was weakly optically scattering, and did not affect significantly the incident speckle. The gel also mechanically mimicked the speed of sound in biological tissue. The first phantom (Phantom 1) contained a cylinder of 5mm in diameter prepared by mixing diluted black ink (Scribtor, Pelikan) with agarose gel to obtain an optical density of 1.5 [Fig 2(a)]. The second phantom (Phantom 2) comprised a 30  $\mu\text{m}$  diameter black-colored nylon suture threads (NYL02DS, 10/0, Vetsuture) arranged in a two-loop knot [Fig 3(a)].

Detection of the photoacoustic waves was performed with a 128-element linear array (Vernon, France) driven by a programmable ultrasound scanner (Aixplorer, Supersonic Imagine). The elements of the array had a center frequency of 20 MHz. They were cylindrically focused at 8 mm and were distributed with a pitch of 80  $\mu\text{m}$ . Water was used for acoustic coupling. Signals were acquired simultaneously on 128 channels at a sampling rate of 60 MS/s for every laser pulse. In each experiment, the measurement sequence consisted of the acquisition of signals corresponding to 50 consecutive laser pulses while continuously rotating the diffuser.

Following each acquisition, the signals were filtered with a 3<sup>rd</sup> order Butterworth bandpass filter between 500 kHz and 25 MHz, and a delay-and-sum beamforming algorithm was used to obtain a dataset of 50 photoacoustic images for the different speckle illuminations. To form the final images, for each pixel  $p$  in the image grid, two statistical quantities were estimated over  $p_i$  ( $i=1..N$ ) pixel values corresponding to  $N$  different realizations of the speckle illumination: its average value and its variability. Specifically, the arithmetic mean  $\mu(p)$  and the Gini mean difference (GMD) were computed. Because of the statistical properties of speckle illumination [7] and the linearity of the beamforming process, the limit of  $\mu(p)$

when  $N$  tends toward the infinity corresponds to the value obtained with a spatially uniform illumination. The statistical dispersion of the  $p_i$  values over  $N$  realizations of the speckle illumination was estimated using the GMD [9]:

$$GMD_N = \frac{\sum_{i=1}^{N-1} \sum_{j=i+1}^N |p_i - p_j|}{N(N-1)/2} \quad (1)$$

The GMD has the advantage over other estimators of the dispersion such as the variance or standard-deviation, that the comparison is done between pairs and it is not defined in terms of a specific measure of central tendency. Moreover, the GMD gives equal weight to all the differences and for speckle illuminations can be computed even for  $N \sim 2$ , when the variance in the mean illumination is large. Photoacoustic reconstructed datasets were normalized by the maximum pixel value before computing the mean image over  $N=50$  realizations of speckle illumination, and the GMD images for  $N=2$  and  $N=50$ . For better visualization of the images, the pixels with values below the most frequent value in the image (mode) were disregarded, and the minimum value was then subtracted to the remaining pixels.

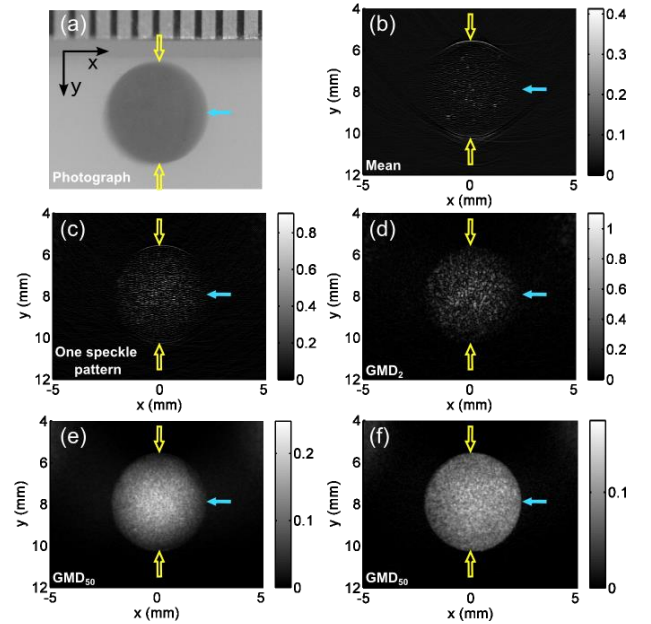


Fig. 2: Images obtained with Phantom 1. (a) Photograph of the  $\varnothing 5\text{mm}$  ink inclusion. A metric ruler was placed on the top for size reference. (b-e) Optoacoustic images from illumination with speckle patterns featuring a grain size of  $2.6\mu\text{m} \pm 0.6\mu\text{m}$ : (b) Mean image over 50 speckle patterns, mimicking a uniform illumination, (c) reconstruction from a single speckle-illumination pattern, (d)  $GMD_2$  image from the illumination pattern in (c) and a second one, and (e)  $GMD_{50}$  image. (f) same as (e) but for grain size of  $6.3\mu\text{m}$ . The superimposed empty and full arrows indicate surfaces respectively parallel and perpendicular to the length axis of the array. GMD images enable to reconstruct a large absorbing structure with a high-frequency photoacoustic system without artifacts.

Fig. 2(b)-2(f) illustrates photoacoustic images obtained with Phantom 1. Because of its shape, size and homogenous absorption, the ink inclusion comprised in Phantom 1 [Fig. 2(a)] is expected to mostly emit ultrasound frequency in the sub-megahertz range when illuminated uniformly [10]. Such frequencies cannot be recorded efficiently with a high-frequency piezoelectric transducer. Therefore, the interior absorption could not be visualized on the mean image [Fig 2(b)], as is the case in conventional photoacoustic imaging. Only the edges facing towards the detector (empty arrows) and a few sparse absorbers, most probably dust particles or large ink particles were visible. The side edges (full arrow) could not be reconstructed because of the limited aperture of the array along the x-axis. However, when illuminated with a speckle pattern, photoacoustic sources could be reconstructed inside the inclusion in addition to the edges [Fig 2(c)]. More sources inside can be visualized when calculating the  $GMD_2$  image, obtained using only two different speckle illuminations [Fig. 2(d)]. This phenomenon can be explained by the heterogeneous spatial distribution of the light intensity [Fig. 1(b)]. Assessing the variability of each pixel over 50 different speckle illumination, the  $GMD_{50}$  image [Fig. 2 (e)] clearly shows that the absorbing inclusion could be visualized and appeared with a uniform brightness, closely reproducing its absorption profile [Fig. 2(a)]. The edges are however not very sharp, but this phenomenon can be attributed to the lower average fluence in the periphery of the inclusion due to the small distance between the diffuser and the sample, that in turn reduced the signal-to-noise ratio for the corresponding pixels, and induced a dispersion similar to the background noise. Placing the diffuser further away increase the illuminated surface and enabled to restore sharp edges and as well as the interior absorption [Fig. 2(f)]. Fig. 2(e) and 2(f) demonstrate that computing GMD images, with even the smallest speckle grain size tested here, enabled to reconstruct a large photo-absorbing structure with a high-frequency photoacoustic system.

Fig. 3(b)-3(f) illustrates photoacoustic images obtained with Phantom 2. The orientation of the black thread in this phantom was chosen to enhance the limited-view problem and to show how speckle illumination can restore visibility for all orientations. Three parts of the thread are visible on the mean image [Fig. 3(b)] (empty arrows): two portions mostly parallel to the x-axis and the top extremity of the thread. All other portions could not be distinguished on Fig. 3(b) and in particular the ones indicated with the full arrows. The images obtained with one speckle illumination [Fig. 3(c)] and  $GMD_2$  [Fig. 3(d)] show that the portions of the thread indicated with the full arrows appear with a granular structure, as if they were formed of discrete absorbers and not a continuous one. Computing the  $GMD_{50}$  image [Fig 3(e)] enable to restore the continuity of the photo-absorbing structure,

and to retrieve the complex shape of the structure [Fig 3(a)]. Similar results could be obtained with the smallest speckle grain size used in this study [Fig. 3(f)], however as for Phantom 1, mainly the parts in the surrounding of the center of the image could be efficiently restored. Fig. 4(e) and 4(f) demonstrate that computing  $GMD_{50}$  images enabled us to reconstruct faithfully all the orientations of a photo-absorbing structure with a limited-view photoacoustic system.

To quantify the effect of the speckle grain size on the reconstructed images, the average variability in pixel value over the realizations of the speckle illumination was assessed, independently of the laser fluence on Phantom 2. This was done by estimating the relative mean difference (RMD) – or Gini ratio – for pixels with a large

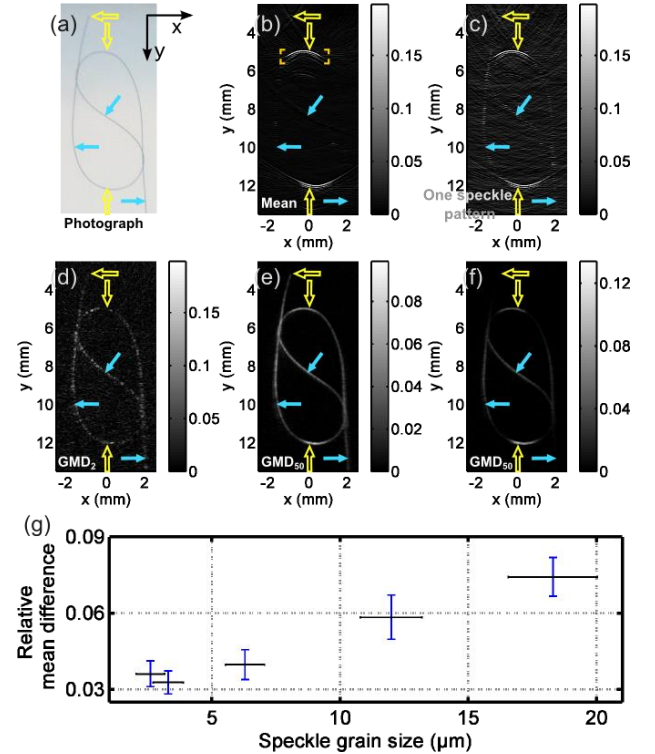


Fig. 3: Images obtained with Phantom 2. (a) Photograph of the Ø30  $\mu\text{m}$  knotted thread. (b-e) Optoacoustic images from illumination with speckle pattern featuring a grain size of  $6.3 \mu\text{m} \pm 0.8 \mu\text{m}$ : (b) Mean image over 50 speckle patterns mimicking uniform illumination, (c) reconstruction from a single speckle-illumination pattern, (d)  $GMD_2$  image from the illumination pattern in (c) and a second one. (e)  $GMD_{50}$  image. (b) and (c) were threshold to the maximum value of (d). (f) same as (e) but for grain size of  $2.6 \mu\text{m} \pm 0.6 \mu\text{m}$ . The superimposed empty and full arrows point out parts of the thread respectively mostly parallel and perpendicular to the length axis of the array. All the orientations of the thread can be retrieved in the GMD images. (g) Averaged RMD values -computed in the area delimited by the superimposed corners in (b)- as a function of the speckle grain size. Vertical error bar: standard deviation, horizontal error bar: estimated precision on the speckle grain size with the camera measurements. The dispersion over the realizations of the speckle illumination decreases with the speckle grain size.

arithmetic mean  $\mu$  (pixels with  $|\mu|$  superior to 3 times the standard deviation of  $\mu$  over all the pixels in the region of interest):

$$RMD = \frac{GMD_{50}}{2|\mu|} \quad (2)$$

The RMD is the analogue of the optical speckle contrast [7] but computed per pixel and on a scale defined by the acoustic resolution. The averaged RMD value quantifies how different two photoacoustic images acquired for two different speckle illuminations will be, and is related to the number of optical speckle grain illuminating optical absorbers in an acoustic pixel [11]. An RMD of zero expresses perfect equivalence in the obtained signals between two uncorrelated speckle illuminations [9] and is expected to occur for sufficiently small speckle grain size compared to the acoustic resolution [2]. An RMD of one expresses maximal inequality among values [9] and is only attainable for optical speckle grain equal or larger than the ultrasound resolution (i.e. speckle contrast equal to 1). Fig. 3(g) shows that the mean RMD value obtained for Phantom 2 increases with the optical speckle grain size but remain well below 1. Here, the speckle grain sizes were at least three times smaller than the acoustic wavelength in water at the low-pass cut-off frequency (25MHz), therefore individual grains cannot be resolved. The two smallest speckle grains, i.e.  $2.6 \mu\text{m} \pm 0.6 \mu\text{m}$  and  $3.3 \mu\text{m} \pm 0.6 \mu\text{m}$ , have very similar mean RMD values. These speckle grains are about 20 times smaller than the smallest measured acoustic wavelength, but still allow image reconstruction.

To conclude, randomly structured illumination using speckle patterns produced by a dynamic scattering medium was demonstrated to compensate for the partial visibility issues in high-frequency photoacoustic imaging. The speckles were generated with a scattering layer at a distance from the sample to allow control of the experimental parameters and because of the relatively short coherence length of the laser employed. To implement the demonstrated technique inside scattering media the coherence length of the laser should be longer than the scattering induced optical path-length differences. In addition, inside scattering tissues the speckle grain size is expected to decrease towards the quasi-constant value of  $\lambda_{\text{laser}}/2$  within depths of the order of the transport mean-free path [12]. For biological tissues and optical wavelength in the near infrared, the transport mean-free path is on the order of 1mm [6]. Assuming that the behavior observed in our experiments depends only on the ratio between the speckle grain size and the acoustic resolution, photoacoustic detection of variation in the speckle illumination at depths larger than 1mm would require either to minimize other sources of variability in measured signals, such as electronic and quantization noise, or to increase the upper cutoff frequency of the ultrasound detection. Recently a

photoacoustic system operating at a low-pass cut-off frequency of 125MHz and reaching depths of at least 5 mm was developed [13]. Dynamic coherent illumination could be suited for this mesoscopic system. At depths shallower than 1mm, optical-resolution photoacoustic microscopic system have been developed [3]. Because of the optical focusing, the spatial extension of the source in the lateral dimension is constrained; however along the depth-of-focus computing the GMD could be useful to retrieve absorbers extended along the axial direction. Speckles grains are expected to be larger at imaging depth of microscopy, and implementations with transducers of center frequency up to 125MHz already exist [14]. Additionally, for *in vivo* biomedical imaging, one may use the natural rapid decorrelation of perfused tissues, which is of the order of a few ms [15], to produce the temporally varying illumination patterns. For our method, complete decorrelation is even probably not necessary and photoacoustic images could be acquired at a high frame rate.

This work was funded by the European Research Council (grant number 278025), the Fondation Pierre-Gilles de Gennes pour la Recherche and the Plan Cancer 2009-2013 (project Gold Fever). O.K. acknowledges the support of the Marie Curie intra-European fellowship for career development (IEF).

## Reference

1. K. P. K. Shung, and G. A. Thieme, Ultrasonic Scattering in Biological Tissues (CRC PressINC, 1993).
2. Z. Guo, L. Li, and L. V. Wang, Medical Physics 36, 4084-4088 (2009).
3. P. Beard, Interface Focus 1, 602-631 (2011).
4. C. Ventalon, and J. Mertz, Opt. Express 14, 7198-7209 (2006).
5. E. Mudry, K. Belkebir, J. Girard, J. Savatier, E. Le Moal, C. Nicoletti, M. Allain, and A. Sentenac, Nature Photonics 6, 312-315 (2012).
6. V. Ntziachristos, Nat Meth 7, 603-614 (2010).
7. J. W. Goodman, J. Opt. Soc. Am. 66, 1145-1150 (1976).
8. Y. Xu, L. V. Wang, G. Ambartsoumian, and P. Kuchment, Medical Physics 31, 724-733 (2004).
9. G. Jasso, American Sociological Review 44, 867-870 (1979).
10. G. J. Diebold, and T. Sun, Acta Acustica united with Acustica 80, 339-351 (1994).
11. T. Chaigne, O. Katz, A. C. Boccara, M. Fink, E. Bossy, and S. Gigan, arXiv:1305.6246 [physics.optics] (2013).
12. R. Pierrat, J.-J. Greffet, R. Carminati, and R. Elaloufi, J. Opt. Soc. Am. A 22, 2329-2337 (2005).
13. M. Omar, J. Gateau, and V. Ntziachristos, Opt. Lett. 38, 2472-2474 (2013).
14. C. Zhang, K. Maslov, J. Yao, and L. V. Wang, Journal of Biomedical Optics 17, 116016-116016 (2012).
15. M. Gross, P. Goy, B. C. Forget, M. Atlan, F. Ramaz, A. C. Boccara, and A. K. Dunn, Opt. Lett. 30, 1357-1359 (2005).